Mon. Not. R. Astron. Soc. **000**, 000–000 (0000) Printed 1 February 2008 (MN LATEX style file v1.4)

The Energetics and Mass-loss of the Dwarf Starburst Markarian 33

Lesley K. Summers[1], Ian R. Stevens[1] and David K. Strickland[2⋆]

[1] *School of Physics & Astronomy, University of Birmingham, Edgbaston, Birmingham, B15 2TT, UK*
lks@star.sr.bham.ac.uk; irs@star.sr.bham.ac.uk

[2] *Department of Physics & Astronomy, The Johns Hopkins University, 3400 North Charles Street, Baltimore, MD 21218, U.S.A.*
dks@pha.jhu.edu

Accepted .....; Received .....; in original form .....

ABSTRACT

We present *ROSAT* HRI X-ray data and optical imaging of the important dwarf starburst Markarian 33. We find an extended, complex, shell-like morphology in the X-ray emission, with an extent of $\sim 2.3 \times 1.9$kpc, coincident with the bright star-forming regions at the centre of the galaxy. The physical extent of this X-ray emission from Mrk 33 is very similar to the observed Hα emission, and suggests that the bulk of the X-ray emission is coming from an expanding superbubble.

We estimate the age and mass of Mrk 33's starburst to be 5.8 Myr and $6.9\times10^6 M_\odot$ respectively with the energy injection rate in the central regions of the galaxy being $\sim 10^{41}$ erg s^{-1}, while the associated mass-loss rate from the star-forming regions is estimated to be $\sim 0.2 M_\odot$ yr^{-1}. We suggest that the X-ray emission is predominantly powered by starburst type activity and argue that a blowout in the form of a galactic wind is the most likely fate for Mrk 33 resulting in the loss of most of the galaxy's metal-enriched material and a small fraction (< 1 per cent) of the ISM.

Key words: ISM: jets and outflows – galaxies: starburst – galaxies: stellar content – stars: Wolf-Rayet – X-rays: galaxies

1 INTRODUCTION

Blue compact dwarf starbursts belong to the group of galaxies which exhibit the starburst phenomenon, of intense star formation lasting for relatively short periods of time ($\leq 10^8$ yr), while having absolute blue magnitudes of $M_B \geq -18$. They are generally low metallicity objects with Z ranging from 1/30 to $1/3 Z_\odot$ (Thuan 1983; Loose & Thuan 1986), which could be the result of metal-loss associated with the bursting nature of their star-formation. Intense periods of star-formation are an important phase of galactic evolution and can have a profound effect on the galaxies in which they occur so the study of local dwarf starbursts can give insight into the fate of similar objects that occurred at high redshifts (e.g. the numerous faint blue compact objects seen on the Hubble Deep Field images, Mobashar et al. 1996). The study of dwarfs is also important as they are the basic building blocks in the hierarchical merging cosmological scenario and as such are likely to have harboured the earliest occurrences of star-formation in the Universe.

The onset of a starburst leads to the formation of OB associations or even super star-clusters (SSCs) containing many massive stars that have strong supersonic stellar winds injecting both energy and mass into the interstellar medium(ISM). After a period of about 3.5 Myr they begin to give rise to core-collapse supernovae which add to both the energy and mass loss from the starburst. The effect of these winds and supernovae is to sweep-up the ISM and produce shock-heating of both ISM and wind material leading to the production of an expanding superbubble of hot gas contained within a shell of cool ISM material. The formation of such a structure will be accompanied by extended X-ray emission from the hot gas ($T \sim 10^6 - 10^7$ K) and optical Hα line-emission from the cooler ($T \sim 10^4$ K) shell. The continued expansion of the superbubble into the halo of the galaxy is due to it having a greater internal pressure than the surrounding ISM. The onset of Rayleigh-Taylor instabilities is likely to lead to the rupture and subsequent escape of the hot gas in the form of a galactic wind, as seen most spectacularly in M82 (Strickland, Ponman & Stevens 1997) and NGC 253 (Strickland et al., 2000). Typical signatures of such an event are spurs of X-ray emission coincident with the Hα emission (Heckman et al. 1995) and horse-shoe shaped Hα emission with the open end furthest from the centre

⋆ *Chandra* Fellow.

of any starburst regions (Marlowe et al. 1995). The optical and X-ray phenomena described here have been observed in several dwarf starburst galaxies. For example, He 2-10 (Méndez et al. 1999), NGC 1569 (Heckman et al., 1995) and NGC 5253 (Strickland & Stevens, 1999). Such scenarios can have a catastrophic effect on their host galaxies if it results in the loss of a significant fraction of their mass, leading to expansion of the galaxy, a drop in its surface brightness and, potentially, a cessation of star-formation. The rupturing of superbubbles, allowing the venting of hot metal-enriched gas will effect the galaxy's chemical composition and evolution. Such blow-outs could explain the low-metallicities observed in dwarf galaxies and because of their large numbers, the mass and energy lost from them during such processes will have had a profound impact on the state of the intergalactic medium (Dekel & Silk 1986).

We present here new observations of Mrk 33 (Haro 2, UGC 5720, Arp 233, IRAS 10293+5439). This blue compact dwarf galaxy (BCDG) with a mass $\sim 10^9$ $M_\odot$ (Loose & Thuan 1986) lies at a distance of 22 Mpc (Conti 1991) assuming $H_0 = 75$ km s^{-1} Mpc^{-1}. At this distance, $1''$ is equivalent to a distance of 0.11 kpc. Mrk 33 does not appear to have any obvious companions however there is a very red galaxian object ($B - R = 1.7$ from the USNO A2.0 Catalogue, Monet, 1998) lying at a projected distance of ~ 30 kpc ($4.7'$) and at a position angle of 63° with respect to Mrk 33's position of $\alpha = 10^h32^m32^s$ and $\delta = +54°24'03.5''$ (J2000). Somewhat closer in projection, Möllenhoff et al. (1992), detected a radio source with no obvious optical counterpart ~ 3.2 kpc ($30''$) north of Mrk 33. As there is no kinematic data available for either of these objects, it is impossible to say whether they have any association with Mrk 33. Described by Huchra (1977) as being, 'patchy with wisps and a high surface brightness', Mrk 33 was later given an nE classification by Loose & Thuan (1985; 1986). Due to its apparently straight-forward morphology, Mrk 33 is the prototype of this class of object and as such gives an interesting and important snapshot of this intriguing phase of galaxy evolution. The galaxy's blue colour is emphasised by its B magnitude ($m_B \sim 13.40$, de Vaucouleurs et al., 1991) and its $(B-V)$ colour of 0.36 (Thuan & Martin 1981), which is bluer than other starburst galaxies (e.g. NGC 5253 $(B-V) \sim 0.44$; NGC 1569 $(B-V) \sim 0.77$; M82 $(B-V) \sim 0.87$ all values quoted are from the Sky Catalogue 2000.0 Vol. 2, (Hirshfeld & Sinnott 1997)). Compared with other BCDGs, which have metallicities $\sim 0.02-0.20$ solar, Mrk 33, with a value of ~ 0.3 solar (Legrand et al. 1997), seems to have a somewhat high value.

Radio observations of Mrk33 show it to have a steep spectrum with a spectral index of $\alpha = -0.82 \pm 0.12$ (Klein et al. 1984), suggesting the presence of non-thermal sources such as supernova remnants. More recent results from Beck et al. (2000) show the presence of both thermal and non-thermal emission with the former coming mainly from the outer regions of the galaxy and not from point sources, while the latter comes mainly from the inner regions. At shorter wavelengths, the far-infrared luminosity of Mrk 33 from $40 - 120\mu$m is $L_{FIR} \sim 1.4 \times 10^{43}$ erg s^{-1} (calculated as the average value quoted from Thuan & Sauvage 1992, Melisse & Israel 1994 and Stevens & Strickland 1998).

Optical and UV observations of Mrk 33 along with spectral synthesis techniques show that the galaxy has experienced at least two other episodes of intense star-formation prior to the current one, (Loose & Thuan 1986; Fanelli et al. 1988). The most prominent emission feature in the optical spectrum is that of the Hα+N[II] blend and Legrand et al.'s (1997) study of this emission line found evidence of a partially ionised wind out-flowing from the star-forming region at ~ 200 km s^{-1}. The Lyα spectrum has a P-Cygni type profile which also contains blue-shifted Lyα emission indicative of the outflow of partially ionised gas at a speed ~ 200 km s^{-1} (Lequeux et al. 1995). Tenorio-Tagle et al. (1999) have predicted such profiles as the result of an expanding ionization front trapped within the recombining shell of an expanding superbubble, when the bubble has an age ~ 5 Myr.

A value for the soft X-ray luminosity of Mrk 33, in the $0.1 - 2.4$ keV band, was obtained from *ROSAT* PSPC data by Stevens & Strickland (1998) in their survey of X-ray emission from Wolf-Rayet galaxies. The value quoted was $L_X = 1.4 \times 10^{40}$ erg s^{-1} resulting from a best fit to the spectrum of a single-temperature Raymond-Smith model with $kT = 0.36$ keV and $N_H = 2.2 \times 10^{21}$ cm^{-2}. The quality of the X-ray spectral data was poor, and to obtain this fit, the metallicity was fixed at 0.1 solar, somewhat lower than the 0.3 solar quoted earlier. Consequently, there are substantial uncertainties in the spectral fit and in particular on the value of N_H. Hence, when the extreme values of N_H were used, the intrinsic X-ray luminosity was only constrained to be in the range $2 \times 10^{39} - 1.4 \times 10^{42}$ erg s^{-1}, although the uncertainty on the observed value will be much less than this range.

In Section 2, we describe the new observations, firstly the X-ray observations with the *ROSAT* HRI instrument and secondly B and R band optical imaging with the 1.0 m Jacobus Kapteyn Telescope (JKT) on La Palma. The results obtained from these observations are detailed in Section 3 while the implications of the optical results and the energetics of the starburst are discussed in Section 4 with a view to determining the mass-loss rate from the starburst region, the energy injection rate into the ISM and their possible implications on the subsequent evolution of Mrk 33. Our main conclusions are summarised in Section 5.

2 OBSERVATIONS AND ANALYSIS

2.1 New HRI Observation

Mrk 33 was observed with the *ROSAT* HRI on April 29^{th} 1997 for 47676s. By using two microchannel plates and a crossed grid position read out system, the HRI produces images at its prime focus with a spatial resolution $\sim 5''$. The low number (16) of pulse height analyzer (PHA) channels mean that its spectral analysis capabilities are limited (David et al., 1995), however it is possible to calculate hardness ratios for objects (See later). The raw data set was obtained from the Leicester Data Archive (LEDAS) and the data analysis was performed using the Starlink ASTERIX X-ray analysis package. After screening for bad data, no correction to the data needed to be made. Two initial images were produced from the data, the first, for point source searching of the entire field, was $0.6° \times 0.6°$ square with the data binned in 5 arcsec square pixels, while the second, for detailed study of the region around Mrk 33, was

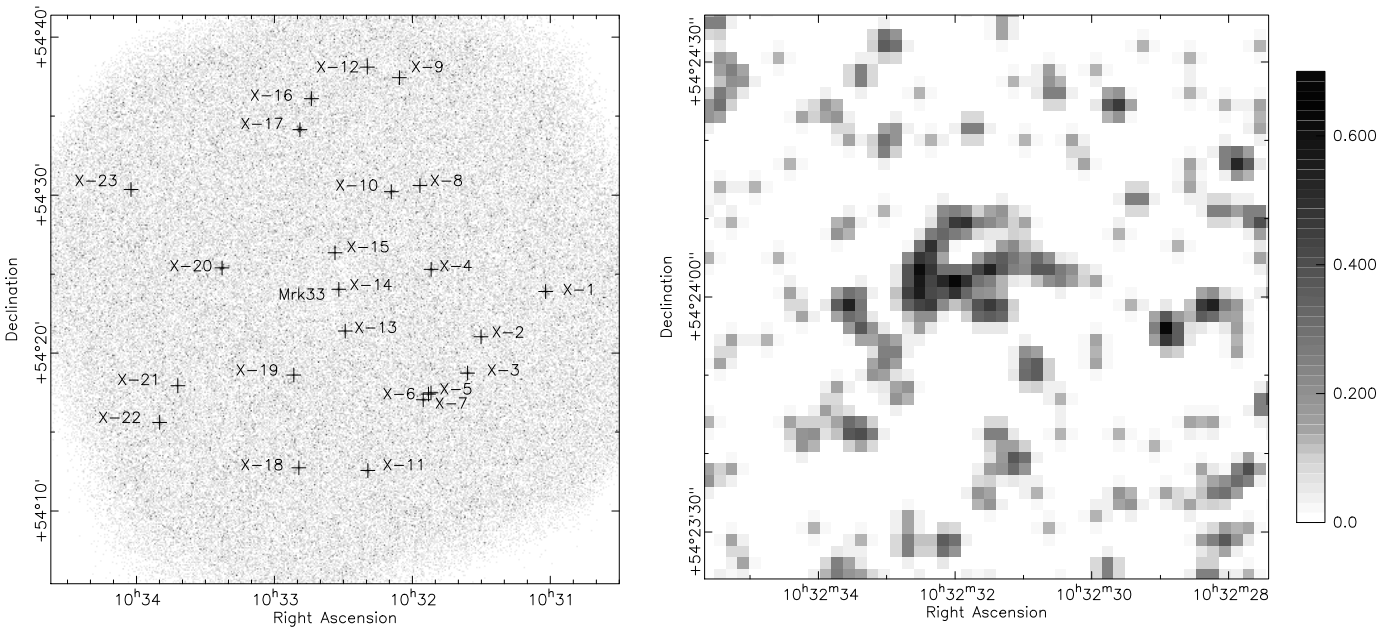

Figure 1. The *ROSAT* HRI data on the Mrk 33 field. Left: A low resolution image of the 47.7ks *ROSAT* HRI observation. The image has been marked with the 23 sources detected with a significance $\geq 4\sigma$ above background. The full listing of these sources is given in Appendix A and their positions are only accurate to within $10''$. Right: A high-resolution, background subtracted, HRI X-ray image of Mrk 33. The key shows the counts pixel^{-1} above the background level. North is to the top and East to the left.

of higher resolution, being $0.2^\circ \times 0.2^\circ$ square with the data binned in 1.5 arcsec square pixels. In both cases, only the photons received in PHA channels 3 - 8 were used so as to reduce the contribution from background sources (e.g. the detector's internal background, the X-ray background and charged particles). A constant background model was constructed for each of these images using a source free annulus with $r = 0.05 - 0.08^\circ$ centred on the centre of the HRI field of view, which lies $\sim 40''$ SSE of Mrk 33. The count rate obtained for each of these background models was $(2.93 \pm 0.25) \times 10^{-3}$ ct s^{-1} arcmin^{-2}. This value was then subtracted from each image and the resulting background subtracted images were then smoothed using a Gaussian with $\sigma = 5''$, in the low resolution case and $3''$ in the high resolution case. The images from both of these procedures are shown in Fig. 1.

2.1.1 Point Source Searching

The ASTERIX maximum likelihood point source searching algorithm, PSS (Allan 1993), was used to detect point sources with a significance greater than 4σ above the background. Although 22 sources, excluding Mrk 33, were detected in the HRI field of view, none of them, within a radius of $20''$, could be identified with known point sources in the SIMBAD database or in the USNO-A2.0 catalogue down to an apparent magnitude of 17.5 (Monet 1998). As a result, no correction could be made for any pointing errors and so the positions of these objects are accurate only to within $10''$ (David et al. 1995). The 23 sources, including Mrk 33, are shown in Fig. 1 superimposed on the low-resolution X-ray image and for completeness, the full listing of all 23 point sources in the field of view is presented in Appendix A.

2.2 New JKT imaging

Mrk 33 was observed using the 1.0 m JKT, on La Palma, on the 2^{nd} January 2000. Seven B band and seven R band images, each with an exposure time of 300s were produced using Harris B and R filters and the *SITe2* CCD. One of the B band images was subsequently rejected because of contamination in the same area of the image as Mrk 33. In addition to these target images, bias frames, flat-fields, and calibration images were also obtained. The images were processed using the IRAF CCD processing software, *ccdproc* in combination with its image processing software, *images*. After bias subtraction and flat-fielding, the target frames were weighted and aligned before being combined. The weighting was achieved using the IRAF digiphot aperture photometry software, *apphot* and the photometric calibration software *photcal*, on the calibration images to find the atmospheric extinction and colour corrections to be applied to each target image. The required standard star magnitudes and colours were taken from the Landolt catalogue (Landolt 1992). The resulting B and R band images are shown in Fig. 2 and Fig. 6 respectively.

3 RESULTS

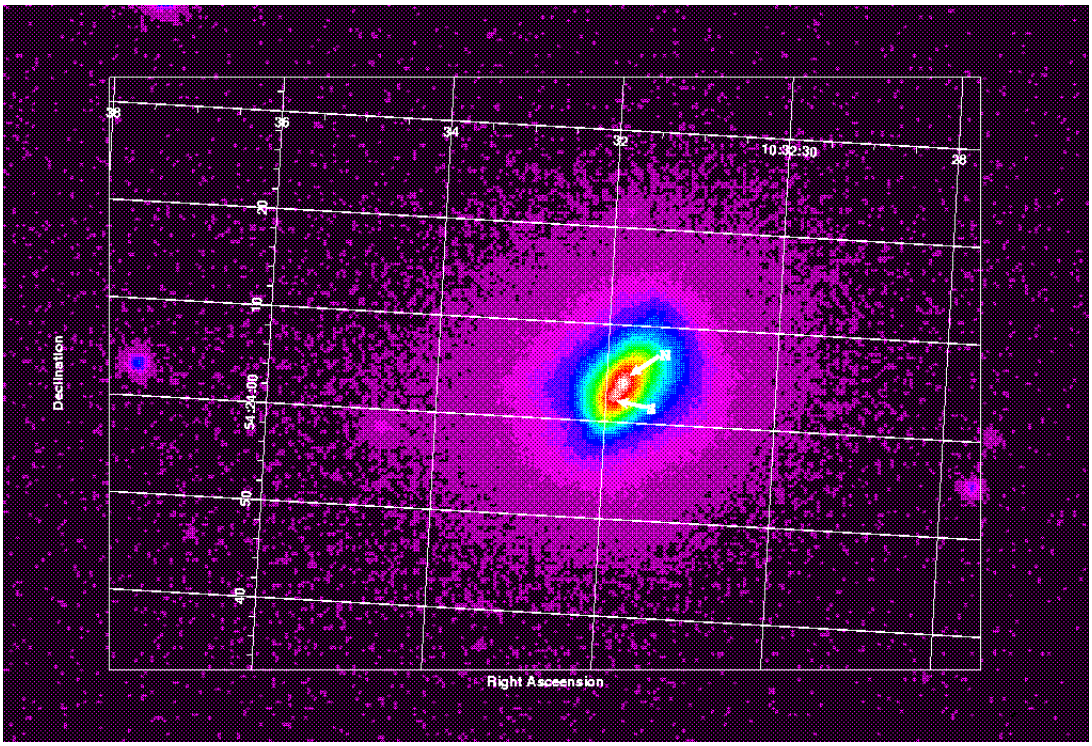

Figure 2. The JKT B band image of Mrk 33 with the two peaks of emission from the star-forming regions labelled N and S.

3.1 JKT Data

The B band image of Mrk 33 shown in Fig. 2 confirms that the intense star-formation occurring in the galaxy is confined to the nuclear region and suggests that the radius of this region's extent is of $\sim 10-15''$ from the peak of the optical emission (corresponding to $\sim 1-1.5$ kpc for an assumed distance of 22 Mpc). In comparison, the low surface brightness extent of the galaxy can be seen to extend out to $\sim 1'$ (~ 6 kpc) in diameter. Fig. 3 shows the counts per pixel for a slice across the B band image running from the NW to the SE of the galaxy from a position of $\alpha = 10^h32^m31^s$ and $\delta = +54°24'16''$ (J2000) to a position of $\alpha = 10^h32^m32.7^s$ and $\delta = +54°23'51''$ (J2000). The image shows 2 peaks of emission, labelled N and S in Fig. 2, occurring at positions of $\alpha = 10^h32^m31.8^s$ and $\delta = +54°24'04''$ (J2000) and $\alpha = 10^h32^m31.9^s$ and $\delta = +54°24'03''$ (J2000) respectively, which are extended over a distance of at least $10''$.

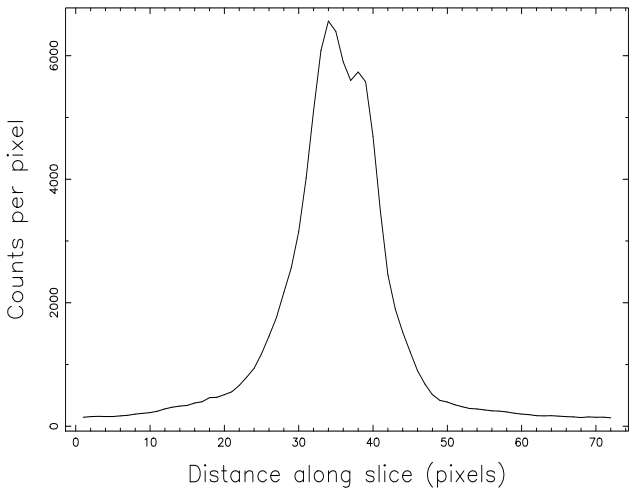

Figure 3. Slice through the blue image of Mrk33 showing the number of counts per pixel in a slice running from NW to SE with 10 pixels = $5''$. The positions of the peaks and the ends of the cut are given in the text.

3.1.1 Surface Brightness Radial Profiles

From the optical images, surface brightness profiles have been obtained using the isophotal plotting capabilities of IRAF. The foreground/background sources that are evident on the B and R band images were subtracted from the images before the fitting of elliptical isophotes was carried out. The ellipses were allowed to vary in both ellipticity (with the ellipticity defined as $e = 1 - b/a$, with a and b the fitted semi-major and semi-minor axes respectively) and position angle, while the ellipse centre was fixed on the optical centre of the most northern of the optical peaks seen on the JKT images.

The B and R band surface brightness profiles are plotted in Fig. 4. Following Loose & Thuan (1996) these have been plotted in three ways. The first plot shows the surface brightness against photometric equivalent radius ($r = \sqrt{ab}$), a plot that is indicative of an exponential law ($I(r) = I_0e^{-ar}$) when giving a straight line and one which is characteristic of a disk system. The best fit lines shown on the plot are for the data with $r > 10''$ and have slopes of -0.057 ± 0.001 and -0.056 ± 0.001 for the blue and red data respectively. The second plot shows surface brightness

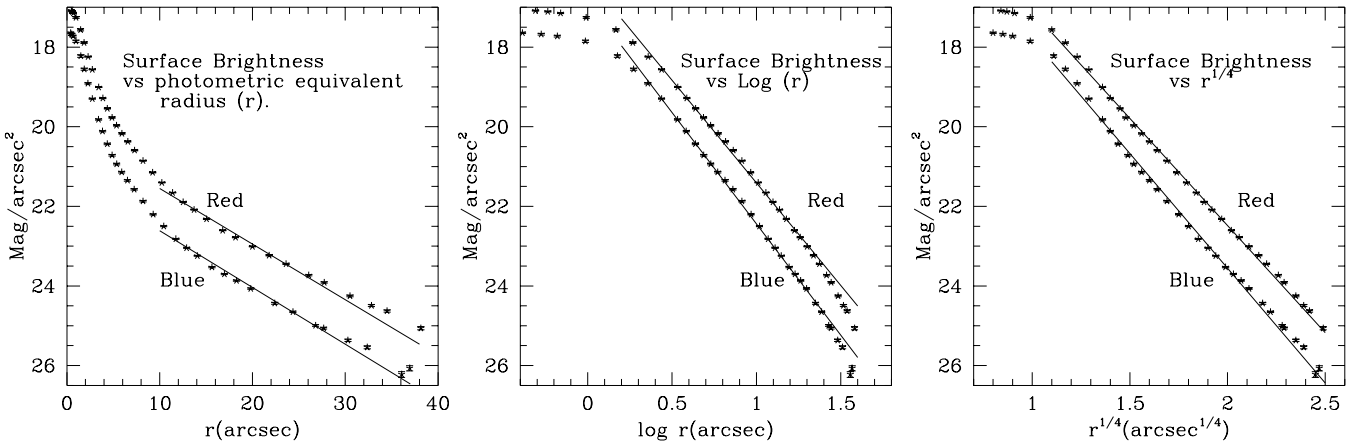

Figure 4. Left: Radial surface brightness profile of Mrk 33 for the JKT B and R band data. Centre: Radial surface brightness profile plotted against $\log r$. Right: Radial surface brightness profile plotted against $r^{1/4}$. Details of the best fit lines are given in the text.

against log (r) where a straight line is indicative of a power law $(I(r) = I_0 r^{-n})$ and the third shows surface brightness against $r^{1/4}$. In the last case, a straight line is indicative of a de Vacouleurs law of the form $I(r) = I_e e^{-7.67[(r/r_e)^{1/4}-1]}$ which is characteristic of spheroidal systems where, r_e is the effective radius containing half the light emitted from the system and I_e is the effective surface brightness at that radius. For the second and third plots in Fig. 4 the best fit lines shown are only for the data with $r \geq 1.5''$. In the log (r) plot, the slopes of the lines are -2.24 ± 0.01 and -2.06 ± 0.01 for the blue and red data respectively. In the case of the $r^{1/4}$ plot they are -2.31 ± 0.01 and -2.15 ± 0.01 again for the blue and red data respectively.

The ellipticity and position angle profiles are shown in Fig. 5. The ellipticity does not show a smooth variation from the centre out but this is probably due to the starburst region affecting the shape of the isophotes in the central region of the galaxy. The position angle steadily increases with radius suggesting an isophotal twist. In addition to these basic profiles, photometry was performed on both images, resulting in apparent magnitudes of $m_B = 13.5$ and $m_R = 12.6$ for an aperture corresponding to a radius of $33''$ and the $B - R$ colour profile was calculated (also shown in Fig. 5). As expected it shows that the galaxy is bluer in the centre than in the outer regions, reflecting the presence of lots of young blue stars in the central starburst region. The uncertainties shown result from the root mean square fluctuation in the intensity of the data in the pixels along the path of each individual elliptical isophot. The implications of these results will be discussed further in Section 4.

3.2 HRI Data

3.2.1 X-ray Contour Plots and Optical Images

X-ray contours from the high resolution X-ray image smoothed using a Gaussian with $\sigma = 3''$ have been overlaid on the R band image of Mrk 33. The resulting image is shown in Fig. 6. The image shows a central extended source of X-ray emission and what could be several point sources of emission lying within a projected distance of $33''$ from its centre at $\alpha = 10^h 32^m 32.2^s$ and $\delta = +54^\circ 24' 03''$. This projected distance was chosen because it is equivalent to the radius of the circular aperture which corresponded to half the average D_{25} value, calculated from Thuan & Martin 1981, Gordon & Gottesman 1981, Loose & Thuan 1986, Melisse & Israel 1994 and Thuan & Sauvage 1992) and used in the optical photometry.

The extended source is of the order of $21''$ (~ 2.3 kpc) in extent when measured from NNW to SSE and of the order of $17''$ (~ 1.9 kpc) in extent from E to W. Fig. 6 shows that as well as being extended, this source appears to have a blobby nature to its emission.

3.2.2 Emission, Flux and Luminosity from Mrk 33's Extended X-ray Source.

The high-resolution image shown in Fig. 1 was used to compare the X-ray photons in channels $3 - 5$ (softest photons) with those in channels $6 - 8$ (hardest photons). No photons were detected from the extended source in channels $6 - 8$ hence it is very soft and the hardness ratio for the region of radius $33''$ centred on the extended source, defined as the number of counts in channels $(6 - 8)/(3 - 5)$, is 0.11 ± 0.05, which is softer than most of the other 22 X-ray sources detected in the HRI field of view (See Appendix A). The count rate for the extended source is $(4.5 \pm 1.0) \times 10^{-4}$ ct s^{-1}, from which the absorption corrected flux and luminosity have been calculated using the W3PIMMS software from LEDAS. For $N_H = 2.2 \times 10^{21}$ cm^{-2}, $kT = 0.36$ keV (Stevens & Strickland, 1998) and our assumed distance of 22 Mpc, the respective values are $(11.1 \pm 2.5) \times 10^{-15}$ erg s^{-1} cm^{-2} and $(21.7 \pm 4.8) \times 10^{38}$ erg s^{-1}.

4 DISCUSSION

4.1 Morphology of Mrk 33

Recent Hα imaging of Mrk 33 (Méndez et al. 2000) has shown the presence of at least three star-forming knots in the centre of the galaxy. These regions are distributed in a line from NW to SE with the largest knot being in the centre and the two most northern peaks being closest together. These two northern star-forming regions are unresolved in

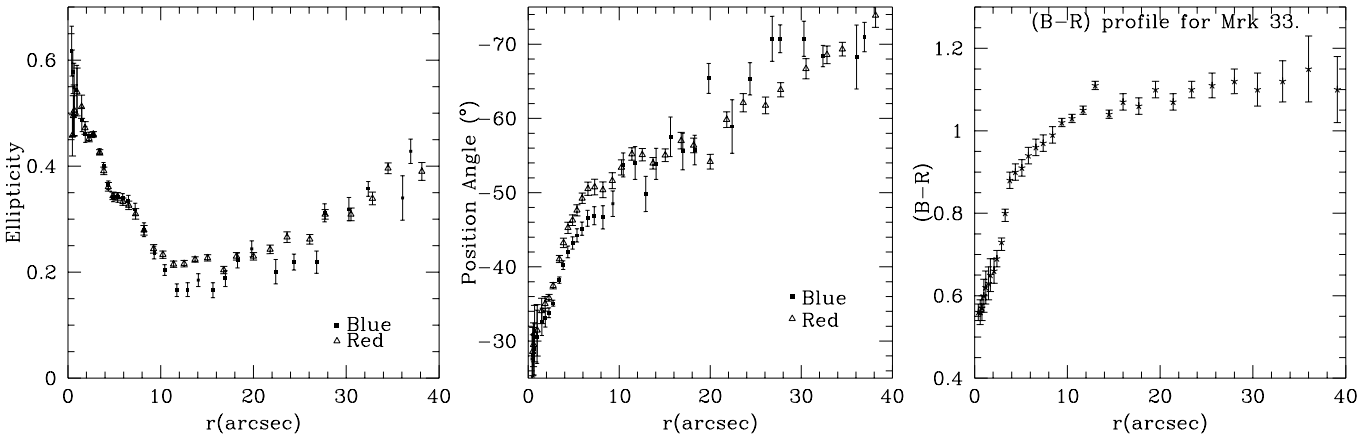

Figure 5. Left: Variation of the ellipticity of Mrk 33, defined as $e = 1 - b/a$, for isophotes out to a radius of 40″ ($\sim$ 4.3 kpc) for both the B and R band observations. Centre: Variation of the position angle of Mrk 33's isophotes also out to a distance of 40″. Right: Variation of the $B - R$ colour of Mrk 33 out to a distance of 40″.

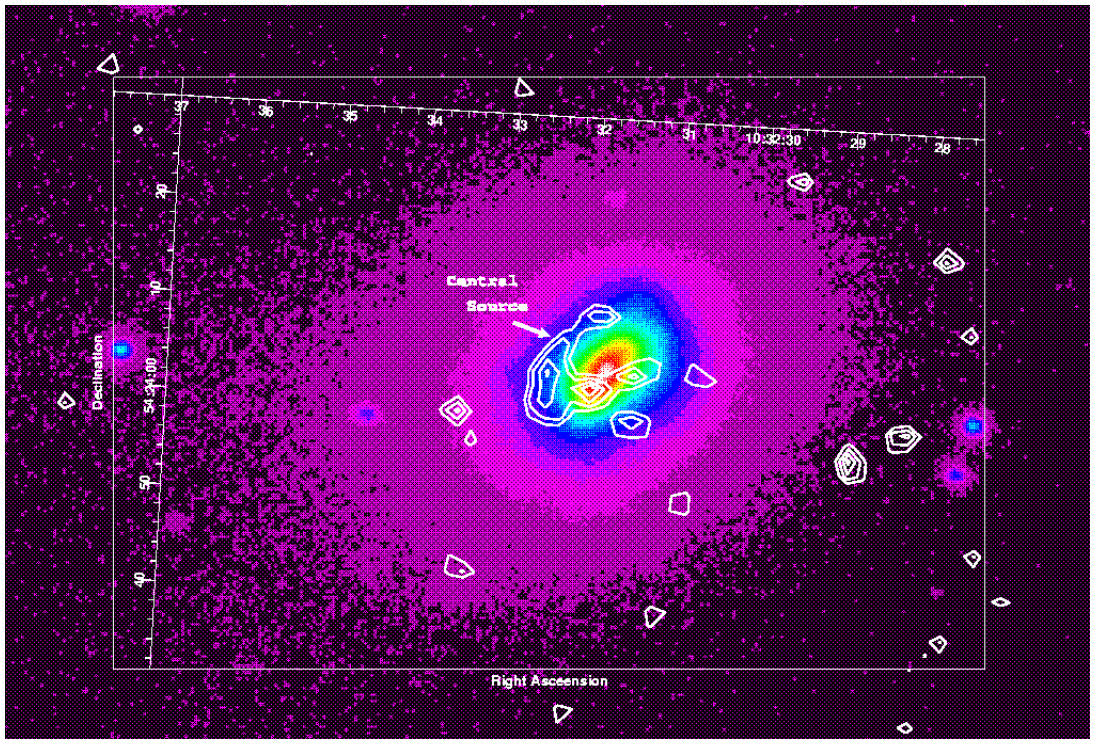

Figure 6. High-resolution X-ray contour image overlaid on the R band JKT image of Mrk 33. The pixel size is 1.5″ smoothed with a Gaussian having a σ of 3″ and the contour levels start at 1.01×10^{-2} ct s^{-1} arcmin^{-2} and increase linearly in steps of 0.33×10^{-2} ct s^{-1} arcmin^{-2}

our optical images and have been labelled N in Fig. 2 whilst the southern one has been labelled S. The region occupied by the three star-forming knots has a size $\sim 7.1'' \times 1.2''$ (380×180 pc at our assumed distance of 22 Mpc) equivalent in area to a circular region of radius $\sim 2.1''$ (~ 225 pc). These sizes correspond well to the inner region with $r < 4''$ that shows the excess light and to the region occupied by the peaks of optical emission shown in Fig. 3. In addition to this, the $R^{1/4}$ fit allows the determination of the half-light radius and the effective surface brightness at this radius. For the blue data these values are 4.35″ and 20.35 mag arcsec^{-2} respectively while the red data gives values of 5.71″ and 20.04 mag arcsec^{-2}. As typical compact dwarfs can be reasonably well fitted by an $R^{1/4}$ law while their diffuse counterparts fit an exponential law best it seems that Mrk 33 is morphologically best described as a compact dwarf elliptical galaxy.

The changes in both Mrk 33's ellipticity and position angle with radius are in reasonable agreement with the results of Loose & Thuan (1986) and Sage et al. (1992). Differ-

ences between our results and those of Loose & Thuan (1986) could have arisen due to the different methods used in ellipse fitting. Our fitting had the ellipse centre fixed on the optical centre of the most northern peak of the two shown on our blue image (Fig. 2) whilst their fitting had the ellipse centre x and y positions as free parameters. The increase in ellipticity seen for radii $\leq 10''$ in our results has been influenced by the linear arrangement of the star-forming knots in the galaxy centre running from NW to SE which will tend to elongate the ellipses.The isophotal twist observed means that our line-of-sight to Mrk 33 is not along any of the galaxy's principle axes. If it were, the isophotes would be aligned like those of an axisymmetric system. It is possible that the twist is the result of the galaxy being triaxial but in no way conclusive. This could only be confirmed if the two true axial ratios could be determined.

4.2 Colour Gradient and Stellar Populations

The $B-R$ colour profile shown in Fig. 5 shows as expected that the galaxy is very blue in the centre and becomes increasingly redder with radius. This reddening is indicative of a change in stellar populations with increasing distance from the centre and is expected from the population synthesis analysis of *IUE* short-wavelength spectra performed by Fanelli et al. (1988). This analysis showed distinct discontinuities in the stellar luminosity function of Mrk 33 with no significant levels of O7–B0V, B2–B9V or supergiants found. The remaining stellar groups of O3–O6V, B1-B1.5V and A0-A7V were detected in increasing numbers and this was interpreted as evidence for Mrk 33 having experienced two episodes of intense star-formation prior to the current one. From the typical ages of the main sequence stars detected, the current burst of star-formation must be around 5 Myr old, the previous one occurred around 20 Myr ago and the earliest one around 500 Myr ago. The fact that the number of stars detected in each group is decreasing with time is indicative of the fact that the amplitude of each successive starburst is also decreasing with time and may suggest that there is less material from which to form stars left after each intense star-forming episode. At a radius $\sim 3.5''$, which would just enclose the star-forming regions, $(B-R) \sim 0.83$, a colour that is typical of an F5V star, and by the time a radius of $\sim 16''$ is reached, this has increased to and levelled out at $B-R \sim 1.1$, typical of a G0V star (Johnson 1966). If these are the oldest stars present then Mrk 33 only started forming stars $\sim 8 \times 10^9$ yr ago.

4.3 Model of a Superbubble

The extended X-ray emitting region in Mrk 33, appears to lie within the expanding Hα shell (diameter ~ 2.8 kpc) observed by Legrand et al. (1997) in the centre of the galaxy, suggesting the presence of a superbubble. The model for such a starburst driven outflow (Castor et al. 1975; Weaver et al. 1977) is outlined below.

Stars of type B2 and earlier have strong stellar winds associated with them, which will deposit $\sim 10^{50}$ ergs of mechanical energy into the ISM, during each star's lifetime. This is of the same order of magnitude as the energy in a supernova shell. As the winds from the OB association of the starburst move out into the interstellar medium, they will sweep up a thin, dense Hα emitting shell. Just inside the shell will be a transition region that is dominated by thermal conduction between the cold shell and the hot (10^7 K) shocked stellar wind inside it. The ionizing of hydrogen is likely to be occurring in the shell itself and outside it there may be a layer of H_2. At first, the wind expands freely into the interstellar medium (ISM) and shocks develop at its leading edge, a strong outward facing shock moving at a speed close to the terminal velocity of the wind and a weaker inward facing shock. As more material is swept up into the region between the two shocks, the momentum of the wind is insufficient to maintain the high speeds and so the shell slows down. This in turn leads to the strength of the inner shock increasing because of the increasing difference between the wind speed and the speed of the shocked material. This free expansion phase is very short and ends when the mass of swept up material becomes greater than the mass deposited in the region between the two shocks by the wind. At this time the gas between the shocks will be very hot with a temperature $\sim 10^7$ K produced by collisions in the shocks converting the mechanical energy of the wind to thermal energy. This thermalisation is particularly efficient because at these temperatures there is little cooling due to radiative losses.

The superbubble then enters its adiabatic phase where it develops an onion-like structure and can be thought of as consisting of five layers (Strickland & Stevens 1999). Layer 1: - A freely expanding supersonic wind bounded by the inward facing shock. Layer 2: - The shocked wind material at $T \sim 10^7$ K. Layer 3: - A contact discontinuity that forms a boundary between the shocked wind material and shocked ISM material. Layer 4: - The hot swept-up shocked ISM material that is bounded by the outward facing shock. Layer 5: - The ambient ISM. Adiabatic cooling occurs as work is being done increasing the bubble's volume and when the point is reached where layer 4's temperature has dropped to $\sim 10^6$ K, the emission of line radiation becomes important and it's temperature rapidly falls to $\sim 10^4$ K. The two phases outlined above are very short, $\sim 10^{-5}\times$ the lifetime of a starburst and so any observed superbubbles are much more likely to be in their third phase which is known as the 'snow-plough phase'.

Layer 2 now occupies most of the bubbles volume and is at a uniform pressure since it is very hot and its sound crossing time is very much less than the age of the bubble. Meanwhile, layer 4 which contains most of the bubble's mass is now a thin, dense, cool shell with its temperature maintained at $\sim 10^4$ K by the UV radiation from the massive stars of the starburst. The bubble continues to expand because its pressure is greater than that of the surrounding ISM and its radius, R_B, and expansion velocity v_B, are given by:

$$R_B = 32.77 \left(\frac{L_{36}}{\mu n_0}\right)^{1/5} t_6^{3/5} \quad \mathrm{pc} \tag{1}$$

$$v_B = 19.28 \left(\frac{L_{36}}{\mu n_0}\right)^{1/5} t_6^{-2/5} \quad \mathrm{km\ s^{-1}} \tag{2}$$

where L_{36} is the mechanical luminosity injected by the starburst in units of 10^{36} erg s^{-1} (the mechanical luminosity injected by a typical B2 star), t_6 is the age of the starburst

in units of 10^6 yr and n_0 is the ambient number density of the ISM.

Thermal conduction at the contact discontinuity leads to the evaporation of material from layer 4 to layer 2 (Weaver et al., 1977), where the balancing of the conductive and mechanical energy fluxes lead to expressions for the temperature, T_2 and the gas density, n_2, at the centre of layer 2 given by:

$$T_2 = 1.77 \times 10^6 \quad \left(L_{36}^8 \, n_0^2 \, t_6^{-6}\right)^{1/35} \quad \mathrm{K} \tag{3}$$

$$n_2 = 0.02 \left(L_{36}^6 \, n_0^{19} \, t_6^{-22}\right)^{1/35} \quad \mathrm{cm}^{-3} \tag{4}$$

Assuming the radiative cooling time is long compared to the expansion time, spherical symmetry, a uniform density ambient ISM and a constant rate of kinetic energy injection then:

$$L_X = \int n(r)^2 \Lambda_X(T, Z) dV \quad \mathrm{erg\ s}^{-1} \tag{5}$$

(Chu & Mac Low 1990) where $\Lambda_X(T, Z)$ is the volume emissivity of the gas over the temperature region being considered. Adopting $\Lambda_X \sim 3{\times}10^{-23} Z$ erg cm^3 s^{-1} for the integral of the volume emissivity over the *ROSAT* HRI energy band (Suchkov et al., 1994; Raymond & Smith, 1977), assuming $r = R_B$ given by equation (1) (since the cool shell is very thin compared with the X-ray emitting region) and taking the radial variation of the density inside the bubble, $n(r)$, to be:

$$n(r) = 1.525 L_{mech}^{6/35} n_0^{19/35} t^{-22/35} \left(1 - \frac{r}{R}\right)^{-2/5} \quad \mathrm{cm}^{-3} \tag{6}$$

(Mac Low & McCray, 1988, following Weaver et al., 1977): where L_{mech} is the mechanical luminosity injected by the starburst and r/R is the fractional radius. Then, integrating over the total bubble volume, L_X is given by:

$$L_X = 7 \times 10^{34} Z L_{36}^{33/35} n_0^{17/35} t_6^{19/35} \quad \mathrm{erg\ s}^{-1} \tag{7}$$

4.4 Application of the model to Mrk 33

To apply the ideas outlined above to Mrk 33, both an estimate of the starburst age and mechanical energy injection rate are required. Legrand et al.'s (1997) measurement of the size and outflow velocity of the Hα shell give values of $r \sim 1.3 - 1.4$ kpc (scaled to a distance of 22 Mpc) and $v = 200$ km s^{-1}. The earlier work of Lequeux et al. (1995) studying Mrk 33's absorption lines of Lyα, OI, NI, SiII, and SiIII also found evidence for an outflow from the galaxy, which was interpreted as a galactic wind with a velocity of ~ 200 km s^{-1}. Adopting this value for the expansion velocity of the superbubble and assuming an average radius of $R_B = 1.1$ kpc (see Section 3.2.1) for the extended X-ray emitting source, a first estimate of the dynamical age, t can be made by taking the ratio of equations (1) and (2):

$$t_6 = 0.59 \frac{R_B(\mathrm{pc})}{v_B(\mathrm{km\ s}^{-1})} \quad 10^6\mathrm{yr} \Rightarrow t = 3.2 \times 10^6 \mathrm{yr} \tag{8}$$

This dynamical age would have to be a lower limit for the starburst age and is most likely an underestimate of it since the non-thermal nature of the radio spectrum implies a substantial number of supernova remnants, suggesting that the starburst age should lie between about 4 Myr and 40 Myr. If, as is possibly indicated by the high expansion velocity, the superbubble has already ruptured then this low value for the dynamical age is a result of the hot gas and bubble shell being accelerated to higher velocities during blow out. Once the bubble has expanded to a radius of the order of the galaxy scale height, its growth along the galaxy's minor axis will start to accelerate leading to the rupture of the superbubble and blow out. If the superbubble has a radius of 1.1 kpc then it has already grown to several scale heights, assuming the scale height is of the order of the half-light blue radius (~ 0.48 kpc), and it is likely that acceleration is underway and that blow out has just occurred.

Substituting the value for the dynamical age back into equation (1), while assuming an average number density for the ambient ISM of $n_0 = 0.3$ cm^{-3} (following Marlowe et al., 1995, who quote this as a typical value for this parameter in dwarf galaxies with recent or on-going star-formation) and 90 per cent H to 10 per cent He, gives a maximum value for the mechanical energy injection rate of: $L_{36} = 2.4 \times 10^5$, or $L_{mech} = 2.4 \times 10^{41}$ erg s^{-1}. The L_{36} figure would suggest that the maximum number of stars that could be present in the starburst would be $\sim 2.4 \times 10^5$, assuming they were all of type B2 and the minimum mass of the starburst would be $\sim 2.35 \times 10^6 M_\odot$.

Comparing these values to the evolutionary synthesis models for an instantaneous starburst (Leitherer & Heckman 1995; Leitherer et al. 1999) with a normal Salpeter IMF with $\alpha = 2.35$, an upper mass cut-off of $100 M_\odot$, a lower mass cut-off of $1 M_\odot$ and allowing for the fact that a metallicity of $0.3 Z_\odot$ is being assumed for Mrk 33, this energy injection rate is higher than would be expected for a $10^6 M_\odot$ starburst at 3.2 Myr and suggests the mass of the starburst is $\sim 2.9 \times 10^7 M_\odot$. A better quantity to consider instead of just the mechanical energy injection rate, L_{mech}, is the ratio of L_{mech} to L_{bol}, where L_{bol} is the bolometric luminosity of the starburst assumed to be $\sim L_{FIR}$ (it is better to use this ratio because it is a mass independent quantity). Assuming $L_{FIR} \sim 1.4 \times 10^{43}$ erg s^{-1}, then $L_{mech} \sim 1.6 \times 10^{40}$ erg s^{-1} at an age of 3.2 Myr and the mass of the starburst region $\sim 1.9 \times 10^6 M_\odot$.

Another estimate of the mass of the star-forming region of Mrk 33 has been made by comparing the spectral energy distribution (SED) of the galaxy to those predicted from SED modelling including single and binary systems (Cervino & Mas-Hesse 1999). This gave an average value of $\sim 9.5 \times 10^6 M_\odot$, assuming an =age of 5 Myr for the starburst. The justifications behind this choice are that Mrk 33 is a Wolf-Rayet galaxy (Kunth & Joubert 1985) suggesting an age of $3 - 7$ Myr. Coupled with this, the Lyα profile of Mrk 33 (Lequeux et al. 1995) is typical of that expected for a 5 Myr old starburst from the evolution models of Tenorio-Tagle et al. (1999). A final mass estimate can be obtained from the number of O3–O6 V stars in the starburst. From Fanelli et al. (1988), the extinction-corrected observed flux requires ~ 7150 O3–O6 V stars (when scaled for different assumed distances). Assuming a Salpeter IMF with an upper mass limit of $120 M_\odot$ to accommodate the O3 stars, this gives a mass of $\sim 9.3 \times 10^6 M_\odot$. From the above considerations, a mass of $10^7 M_\odot$ is going to be assumed for the mass of the star-forming region of Mrk 33 and all other quantities will be scaled accordingly.

Table 1. Estimates of the mechanical energy injection rate for Mrk 33 for the six age estimates detailed in the text. Column 2 gives the value calculated by using equation (1) and a value for the radius of the superbubble of 1.1 kpc. Column 3 uses the L_{mech}/L_{bol} ratios from the starburst evolutionary synthesis models (Leitherer & Heckman 1995; Leitherer et al. 1999), assuming L_{bol} for Mrk 33 to be $\sim 1.4 \times 10^{43}$ erg s^{-1}.

Age (Myr)	Calculated L_{mech} (erg s^{-1})	L_{mech} from L_{mech}/L_{bol} (erg s^{-1})
3.2	2.4×10^{41}	1.6×10^{40}
4.5	2.2×10^{41}	1.1×10^{41}
5.0	1.6×10^{41}	1.1×10^{41}
5.9	9.6×10^{40}	1.2×10^{41}
6.0	9.1×10^{40}	1.1×10^{41}
7.5	4.8×10^{40}	1.5×10^{41}

An upper limit on the age of the starburst is suggested by the $B-R$ colour of Mrk 33 in its central region. The value of 0.56 shown in Fig. 5 would correspond to an age of 7.5 Myr from the evolutionary synthesis models but the actual value of $B-R$ in the central region is likely to be bluer than this due to the presence of large numbers of O and B stars and the fact that the surface brightness has not been determined using elliptical isophotes that just include the star-forming regions.

The flux in the Hβ line found in Mrk 33's spectrum is predominantly produced by the massive ionizing stars found in the star-forming regions. The equivalent width of this line, which decreases with time as the number of hot stars decreases, is therefore a measure of the relative number of these stars in the galaxy and hence also an age indicator. For Mrk 33, typical values of 21Å (Kennicutt 1992), 23Å (Conti 1991) and 30Å (Mas-Hesse & Kunth 1999) have been quoted and these would correspond to ages of ~ 6, 5.9 and 5 Myr respectively, from evolutionary synthesis models. It is possible that these could be underestimates though as no allowance has been made for the presence of binary stars in the galaxy, which would tend to increase the age at which a particular equivalent width of Hβ occurs at least for starbursts older than 4 Myr (Van Bever & Vanbeveren 1998). Also, the total number of photons below the Lyman limit can be used as an age estimator. For Mrk 33, this quantity has a value of 2.5×10^{52} photons s^{-1} (Conti 1991) which would correspond to an age of ~ 4.5 Myr.

Table 1 gives the estimates of L_{mech} calculated using equation (1) and also those determined from the L_{mech} to L_{bol} ratio for the six age estimates discussed above. The values obtained from the dynamical age differ by more than an order of magnitude and so both for this reason and the reasons given earlier, these results will not be included in the subsequent analysis.

The average age and mechanical energy injection rate from the remaining estimates are 5.8 ± 1.0 Myr and $(1.2 \pm 0.2) \times 10^{41}$ erg s^{-1} respectively. Using these values in equations (1) and (2) give $R_B = 1.4 \pm 0.2$ kpc and $v_B = 139 \pm 18$ km s^{-1} respectively, which are in reasonably good agreement with the observations. The fact that the expected expansion velocity is less than that observed supports the idea that acceleration may be occurring. Compared with the evolutionary synthesis models, the figures would suggest a mass for the starburst of $\sim 3.8 \times 10^6 M_\odot$. Another and probably more reliable estimate of the mass of the starburst region can be obtained from comparing the absolute blue magnitude of the starburst region with the values predicted from the evolutionary synthesis models (Leitherer et al. 1999). Assuming the starburst is confined to the central region within a radius of $10''$ then aperture photometry gives an apparent blue magnitude, $m_B = 13.8$ and an absolute blue magnitude, $M_B = -17.9$ for this region. This value of M_B is ~ 2.1 magnitudes brighter than predicted for a $10^6 M_\odot$ starburst at an age of 5.8 Myr and implies that the mass of the starburst is $\sim 6.9 \times 10^6 M_\odot$. From this result, the assumption of a mass of $10^7 M_\odot$ for the starburst is not unreasonable.

Utilising equations (3) and (4) above along with the average age and mechanical energy injection rates just determined, the temperature and number density at the centre of layer 2 of the superbubble would be: $T_2 = (1.77 \pm 0.19) \times 10^7$ K and $n_2 = (0.026 \pm 0.004)$ cm^{-3} respectively assuming $n_0 \sim 0.3$ cm^{-3} as stated earlier. This temperature is somewhat higher than that obtained from the spectral fitting of Stevens & Strickland (1998) where a value of $kT = 0.36$ keV was quoted. This is to be expected however as the conductive evaporation and mixing of denser gas from layer 4 with the more tenuous gas of layer 2 just behind the contact discontinuity will cause T to drop rapidly here since nT is constant. The temperature T_2 on the other hand corresponds to the temperature of the gas at the centre of layer 2 just after it has been shock heated and assumes 100 per cent efficiency in the thermalizing of the mechanical energy represents a maximum value for the X-ray temperature.

The model would predict that the X-ray luminosity, given by equation (7) and assuming a metallicity of $0.3 Z_\odot$ for Mrk 33 should be: $L_X = (1.8 \pm 0.4) \times 10^{39}$ erg s^{-1}. This value is comparable to that measured for the X-ray luminosity of the extended central source.

4.5 Other Sources of X-ray Emission

The discussion in Section 4.4 shows that the extended X-ray source in the centre of Mrk33, when treated as a whole, can be modelled as a superbubble. However, as this source has a blobby structure to its emission, there are other possibilities and as in all galaxies, the X-ray emission seen in Mrk 33 will come form a combination of sources which will contribute in varying degrees to the overall observed flux.

Massive O stars will typically contribute around $10^{31} - 10^{32}$ erg s^{-1}each to the X-ray luminosity (Sciortino et al. 1990) giving around $10^{35} - 10^{36}$ erg s^{-1} in total, while lower mass stars with $L_X \sim 10^{-3} L_{Bol}$ (Stocke et al. 1991) will contribute a similar amount. In total this is $< 1\%$ of the emission from the extended central source. X-ray binaries while giving an adequate luminosity would appear as point sources and also would have a harder spectrum than is observed in Mrk33 (Read, Ponman & Strickland 1997). Supernova remnants have the right temperature spectrum (Read, Ponman & Strickland 1997) and the steep radio spectrum of Mrk33 is indicative of the presence of such sources (Klein et al 1984). However, the size of the extended source is $\sim 10 - 100$ times the size of typical supernova remnants and several hundred would be required in a very small volume to give the nec-

essary luminosity. The short lived nature of Type II supernovae and the need for them to occur in very dense mediums (Schlegel 1995) or close to superbubble shell walls (Chu & Mac Low 1990) to produce the required luminosity means that they too are unlikely to be responsible for most of the observed X-ray emission.

From the above considerations it seems most likely that the main contribution to the X-ray emission from the extended central source is from shock-heated gas within one or more superbubbles. Improved spatial resolution observations with say the Chandra HRC would be useful in order to decide whether or not there are any point-like sources in the region.

4.6 The Long Term Effects on Mrk 33

The fate of a dwarf galaxy experiencing a starburst depends on what happens to the accelerated material from its ISM and that ejected from its stars. In essence, there are three possible outcomes to the superbubble scenario.

Firstly, the ambient ISM could be accelerated to a speed beyond the escape velocity of the galaxy and expelled along with the mass ejected in the form of stellar winds and supernova ejecta. Modelling carried out by De Young & Heckman (1994) shows that the most likely situation to result in total loss of the ISM is a thick, low-density disk being subjected to a high energy injection rate. For a $10^9 M_\odot$ galaxy with a semi-major axis of 3 kpc and an impulsive energy injection of 10^{55} erg, they find that the ISM will only be lost if it has a density of less than 0.1 cm^{-3} and a semi-minor axis grater than 1 kpc. These figures are not dissimilar to those of Mrk 33 but its ISM is probably denser and although the total kinetic energy injected during the starburst is $\sim 10^{55}$ erg, this energy has not been injected impulsively hence, not all of the ISM is likely to be lost in the current starburst. This is supported by estimates of the escape velocity for material at the current radius of the shell of the superbubble. Modelling the potential of the galaxy as a simple spherically symmetric truncated isothermal potential (Binney & Tremaine 1987), as has been done by several authors when modelling dwarf galaxies (e.g. Marlowe et al. 1995; Martin 1999), the escape velocity for material at a distance r from the centre is given by:

$$v_{esc}(r) = 2^{1/2} v_{rot}[1 + ln(r_t/r)]^{1/2} \quad \text{km s}^{-1} \tag{9}$$

where v_{rot} is the maximum rotation velocity of the galaxy in km s^{-1} and r_t is the radius at which the potential of the galaxy is truncated.

In the case of Mrk 33, data for the rotation curve is unavailable and the extent of its HI halo is also unknown, but some estimates can be made based on data for other dwarf galaxies. A minimum distance for r_t can be set at the distance where the optical luminosity of the galaxy appears to drop to that of the sky, i.e. $\sim 50''$ or 5.5 kpc. The work of Viallefond & Thuan (1983), reviewing interferometric maps of BCDGs suggests that their HI diameters could be up to 5 times larger than their optical diameters. Setting this as an upper limit gives $r_t = 27.5$ kpc. Substituting these values into equation (9) for material at a distance of 1.1 kpc form the galaxy centre gives:

$$2.28 v_{rot} \leq v_{esc}(r) \leq 2.90 v_{rot} \quad \text{km s}^{-1} \tag{10}$$

For the swept-up shell of ISM, expanding at 200 km s^{-1}, to escape, the maximum rotation velocity must be less than 70 km s^{-1}. This seems a little lower than most of the rotation speeds for the sample of galaxies discussed by Martin (1999). The acquisition of an HI rotation curve for this galaxy would be particularly useful for determining both the HI extent and escape velocity.

The second and more likely outcome for Mrk 33 is that a blow-out will occur where the bubble ruptures due to the onset of Rayleigh-Taylor instabilities allowing the hot metal-enriched gas to escape from the fragmented shell. Any further hot gas injected by the starburst can then vent directly out of the galaxy, provided its sound speed is greater than the escape velocity. In the absence of radiative cooling, gas hotter than $T_{esc} = 1.5 \times 10^5 (v_{100})^2$ K will escape the galaxy's potential (Martin 1999). Where T_{esc} is the temperature required for the gas to exceed the galaxy's escape velocity and v_{100} is the escape velocity in units of 100 km s^{-1}. Applying this to the gas in layer 2 of the superbubble, at a temperature of $\sim 1.8 \times 10^7$ K, shows that this gas could escape provided $v_{esc} < 1100$ km s^{-1}, which will undoubtedly be the case. This then raises the question of when the superbubble in Mrk 33 is likely to become unstable. The perturbations which give rise to the fractures need time to grow and this growth occurs on a timescale given by Heckman et al. (1995) as:

$$t_{R-T} \sim \sqrt{\frac{\Delta r_{bubble}}{2\pi g}} \sim \sqrt{\frac{\Delta r_{bubble} t_{exp}}{2\pi v_B}} \tag{11}$$

where in this case, g is the net acceleration of the shell (the bubble expansion velocity divided by the expansion time), and Δr_{bubble} is the thickness of the shell. Taking a typical shell thickness of 0.1 kpc, this gives a time of 6.7 Myr for Mrk 33 and suggests that bubble rupture is likely relatively soon and may already have occurred as this value is within our error estimates on the age of the starburst. This scenario is also supported by the work of Mac Low & McCray (1988). They define a criteria for blowout that is based on the parameter Λ, the dimensionless rate of kinetic energy injection given by:

$$\Lambda = 10^4 L_{mech,41} H_{kpc}^{-2} P_4^{-3/2} n_0^{1/2} \tag{12}$$

where $L_{mech,41}$ is the mechanical energy luminosity in units of 10^{41} erg s^{-1}, H_{kpc} is the galaxy scale height in kpc and P_4 is the initial pressure of the ISM in units of $P/k = 10^4$ K cm^{-3}. The condition specified for blowout is that $\Lambda > 100$. Approximating H_{kpc} to the half-light blue radius and $P_4 \sim 1$ then for Mrk 33, $\Lambda \sim 3 \times 10^4$, thus, blowout would appear to be extremely likely.

The third option is that the superbubble could decelerate and stall resulting in radiative cooling and dissipation. If the onset of Rayleigh-Taylor instabilities is as imminent as the above calculations would suggest then there will not be enough time for this last scenario to occur since the winds of massive stars and their supernova explosions will still be occurring to maintain the excess pressure and continued expansion of the superbubble.

As blow-out seems the most likely, it is worth considering how much mass has been deposited in the superbubble and hence how much is likely to be lost from the galaxy when the shell ruptures. A first estimate of the mass deposition rate, $\dot{M}$ for a $10^7 M_\odot$ starburst, with $Z = 0.3 Z_\odot$ and

$t = 5.8$ Myr can be obtained from the starburst evolutionary synthesis models (Leitherer & Heckman 1995; Leitherer et al. 1999), and gives $\dot{M} \sim 0.17 M_\odot$ yr^{-1}. Another estimate can be obtained from the fact that for an adiabatic superbubble, the X-ray temperature, $T_X \sim 5/11 T_0$, where

$$T_0 = \frac{2}{3}\left(\frac{L_{mech}}{\dot{M}}\right)\frac{\mu m_H}{k} \quad \mathrm{K} \tag{13}$$

(Heckman et al. 1995) and is the temperature attained if all the mechanical energy injected by the starburst remains entirely in layer 2. For $T_X \sim 1.77 \times 10^7$ K, a value of $\dot{M} \sim 0.24 M_\odot$ yr^{-1} is obtained, in reasonably good agreement with the first estimate. Hence the average mass loss rate from the starburst in the centre of Mrk 33 is $\dot{M} \sim 0.2 M_\odot$ yr^{-1}.

Finally, the density of the gas in layer 2 can give an estimate of the mass deposited there during the lifetime of the superbubble from both the starburst and conductive evaporation of ISM material from layer 4. This figure will of course depend on the filling factor of layer 2, but assuming no dense clouds are present giving a filling factor is 1, an upper limit for the deposited mass can be obtained. A second assumption is that the radius of the X-ray emitting region is equivalent to the radius of layer 2, R_2, and that any volume occupied by freely expanding wind is very small compared to the volume of layer 2. Hence, with all symbols having their usual meanings and the subscript 2 referring to values within layer 2,

$$M_2 = \rho_2 V_2 = n_2 \mu m_H \frac{4}{3}\pi R_2^3 = 2.2 \times 10^6 M_\odot \tag{14}$$

This mass has been deposited in a time of 5.8×10^6 yr and so for a constant injection rate would imply $\dot{M} \sim 0.38 M_\odot$ yr^{-1}. If the mass loss rate from the starburst is assumed to be $\sim 0.2 M_\odot$ yr^{-1} then this would imply that the rate at which mass is deposited in layer 2 by conductive evaporation of ISM material from layer 4 is $\sim 0.18 M_\odot$ yr^{-1}. If the superbubble was to rupture at around 6.7×10^6 yr then assuming the mass is deposited at a constant rate from both sources, the superbubble would contain a total mass of $\sim 2.5 \times 10^6 M_\odot$, which would be expelled from the galaxy in the form of a galactic wind. Assuming this mass loss rate continues for at least 10^7 yr then around $4 \times 10^6 M_\odot$ of material could be lost from Mrk 33. While this is of the same order of magnitude as the mass of the starburst region, it is only ~ 0.5 per cent of the total mass of the galaxy. It appears likely then that Mrk 33 can survive this starburst episode, just as it has survived its previous two, with most of its ISM intact for use in subsequent star-formation.

4.7 Similar Stories in Other Dwarf Galaxies

Mrk 33, like NGC 5253 is a dwarf starburst where the extended soft X-ray emission seems to be confined well within the galaxy's optical extent and within the observed Hα emission. These two galaxies have probably not yet experienced blow-out of their current superbubbles. In contrast, NGC 1569 shows spurs of X-ray emission (Heckman et al. 1995) which are coincident with its Hα emission, a sign which is indicative of a blow-out having occurred. The age estimate for NGC 1569 is $\sim 10^7$ yr and so it would appear to be an older and more evolved starburst than either Mrk 33 or NGC 5253. NGC 1569 shows evidence for several large kpc-scale structures containing diffuse X-ray emission while Mrk 33 and NGC 5253 have extended regions of X-ray emission that have a blobby structure. All three of these galaxies show evidence for having several distinct star-forming regions present in their starbursts and each region will be responsible for a superbubble. The combination of several superbubbles in this way will give rise to the extended, complex, shell-like morphologies observed in these galaxies. The fact that the superbubbles in NGC 1569 are more easily distinguished from each other than the blobs in the other two galaxies is to be expected if it is older and has therefore had more time to develop its superbubbles.

5 SUMMARY AND CONCLUSIONS

In summary, we have presented a detailed X-ray/optical analysis of the important dwarf elliptical starburst galaxy Mrk 33. We find an extended and complex X-ray morphology associated with the starburst region, and we interpret this emission as being due to a superbubble or outflow being inflated by the starburst. Consideration of the dynamics of the situation show that Mrk 33 is a fairly young starburst galaxy with an age of $t = (5.8 \pm 1.0) \times 10^6$ yrs and that the rate of injection of kinetic energy from the starburst region responsible for inflating the superbubble is $L_{mech} = (1.2 \pm 0.2) \times 10^{41}$ erg s^{-1}. The mass of the starburst region is estimated to be $\sim 7 \times 10^6 M_\odot$. In the superbubble, the temperature of the X-ray emitting gas at the centre of layer 2 is $T = (1.77 \pm 0.19) \times 10^7$ K while its density is $n = 0.026 \pm 0.004$ cm^{-3}. Assuming a filling factor of 1 for this gas, we estimate that the mass deposited in the superbubble from both the starburst region and conductive evaporation of the ISM at the contact discontinuity is $M \sim 2.2 \times 10^6 M_\odot$ and for the age given above, this gives a mass injection rate of $\dot{M} = 0.38 M_\odot$ yr^{-1} of which, ~ 50 per cent comes from the stars of the starburst in the form of stellar winds and supernova ejecta and the remainder is the result of conductive evaporation of the swept-up ISM. It seems most likely that Mrk 33's superbubble will become Rayleigh-Taylor unstable and rupture (in fact the high expansion speed seen in this galaxy may indeed indicate that this has already occurred). The resulting venting of the hot material from within it in the form of a galactic wind will remove ~ 0.5 per cent of the total mass of the galaxy and inject both energy and metal-rich material into the intergalactic medium while allowing Mrk 33 to retain enough of its ISM to continue star-formation in the future.

ACKNOWLEDGEMENTS

LKS and IRS acknowledge funding from a PPARC studentship and Advanced Fellowship respectively. DKS is supported by NASA through *Chandra* Postdoctoral Fellowship Award Number PF0-10012, issued by the *Chandra* X-ray Observatory Center, which is operated by the Smithsonian Astrophysical Observatory for and on behalf of NASA under contract NAS8-39073. The data analysis was performed on the *Starlink* node at Birmingham University. This research has made use of data obtained from the Leicester Database and Archive Service at the Department of Physics

and Astronomy, Leicester University, UK. This research has also made use of the SIMBAD database, operated at CDS, Strasbourg, France. The JKT data analysis made use of the IRAF package, which is distributed by NOAO, which is operated by AURA, Inc., under cooperative agreement with the NSF.

APPENDIX A: POINT SOURCES.

Table A1 lists all 23 sources detected with a significance greater than 4σ above the background in the *ROSAT* HRI field of view during the 47.7 ks observation of Mrk 33. The table is set out as follows: Column 1 gives the source numbers that identify the sources on Fig. 1; Column 2 gives the R XJ name of each source according to the *ROSAT* naming convention (Zimmermann et al. 1997); Columns 3 and 4 contain the right ascension (J2000) and declination (J2000) of the sources respectively where these positions are only accurate to within $10''$; Column 5 lists the significance of each detection in terms of the number of σ above background; Column 6 gives the count rate for each source in units of 10^{-4} ct s^{-1}; and Column 7 gives the hardness ratio ($HR =$ counts in channels $(6-8)/(3-5)$) for each source.

REFERENCES

Allan D. J., 1993, ASTERIX User Note No. 4.
Beck S. C., Turner J. L., Kovo O., 2000, ApJ, 120, 224.
Binney J., Tremaine S., 1987, Galactic Dynamics (Princeton: Princeton University Press.)
Castor J., McCray R., Weaver R., 1975, ApJ, 200, L107.
Cervino M., Mas-Hesse J. M., 1999, in *Wolf-Rayet Phenomena in Massive Stars and Starbursts, IAUS 193*, ed. K. A. van der Hucht, G. Koenigsberger, P. R. J. Eenens. (Calif.: Astronomical Society of the Pacific.), p592.
Chu Y-H., Mac Low M-M., 1990, ApJ, 365, 510.
Conti P.S., 1991, ApJ, 377, 115.
David L. P., Harnden Jr. F. R., Kearns K. E., Zombeck M. V., 1995, The *ROSAT* High Resolution Imager (HRI), US *ROSAT* Science Data Centre/SAO.
Dekel A., Silk J., 1986, ApJ, 303, 39.
De Young D. S., Heckman T. M., 1994, ApJ, 431, 598.
Fanelli M. N., O'Connell R. W., Thuan T. X., 1988, ApJ, 334, 665.
Gordon D., Gottesman S. T., 1981, AJ, 86, 161.
Heckman T. M., Dahlem M., Lenhert M. D., Fabbiano G., Gilmore D., Waller W. H., 1995, ApJ, 448, 98.
Hirshfeld A. & Sinnott R. W., 1997, Sky Catalogue 2000.0 Vol. 2, (Sky Publishing Corporation, C.U.P.).
Huchra J. P., 1977, ApJS, 35, 171.
Inoue H., 1991, in *Frontiers of X-ray Astronomy.*, ed. Tanaka Y., Koyama K., (Tokyo: Universal Academic Press.), p291.
Johnson, H. L., 1966, ARA&A, 4, 192.
Kennicutt Jn. R. C., 1992, ApJ, 388, 310.
Klein U., Wielebinski R., Thuan T. X., 1984, A&A, 141, 241.
Kunth D., Joubert M., 1985, A&A, 142, 411.
Landolt A. V., 1992, AJ, 104, 340.
Legrand F., Kunth D., Mas-Hesse J. M., Lequeux J., 1997, A&A, 326, 929.
Leitherer C., Heckman T. M., 1995, ApJS, 96, 9.
Leitherer C., Schaerer D., Goldader J. D., González Delgado R. M., Robert C., Kune D. F., 1999, ApJS, 123, 3.
Lequeux J., Kunth D., Mas-Hesse J. M., Sargent W. L. W., 1995, A&A, 301, 18.
Loose H-H., Thuan T. X., 1985, in *Star-Forming Dwarf Galaxies and Related Objects*, ed. D. Kunth, T. X. Thuan, T.T. Van (Paris: Editions Frontiéres), p. 105.
Loose H-H., Thuan T.X., 1986, ApJ, 309, 59.
Mac Low M. M., McCray R., 1988, ApJ, 324, 776.
Marlowe A. T., Heckman T. M., Wyse R. F. G., Schommer R., 1995, ApJ, 438, 563.
Martin C. L., 1999, ApJ, 513, 156.
Melisse J. P. M., Israel F. P., 1994, A&AS, 103, 391.
Méndez D. I., Esteban C., 2000, A&A, 359, 493.
Méndez D. I., Esteban C., Filipovic M. D., Ehle M., Harberl F. Pietsch W., Haynes R. F., 1999, A&A, 349, 801.
Mobashar B., Rowan-Robinson M., Georgakakis A., Eaton N., 1996, MNRAS, 282, L7.
Möllenhoff C., Hummel E., Bender R., 1992, A&A, 255, 35.
Monet D. G., 1998, BAAS, 193, 120.03.
Raymond J. C., Smith B. W., 1977, ApJS, 35, 419.
Read A. M., Ponman T. J., Strickland D. K., 1997, MNRAS, 286, 626.
Sage L. J., Salzer J. J., Loose H-H., Henkel C., 1992, A&A, 265, 19.
Schlegel E. M., 1995, Rep. Prog. Phys., 58, 1375.
Sciortino S., Vaiana G. S., Harnden F. R., Ramella M., Morossi C., Rosner R., Schmitt J. H. H. M., 1995, ApJ, 361, 621.
Stocke J. T., Morris S. L., Gioia I. M., Maccacaro T., Schild R., Wolter A., Fleming T. A., Henry J. P., 1991, ApJS, 76, 813.
Stevens I. R., Strickland D. K., 1998, MNRAS, 294, 523.
Strickland D. K., Ponman T. J., Stevens I. R., 1997, A&A, 320, 378.
Strickland D. K., Stevens I. R., 1999, MNRAS, 306, 43.
Strickland D. K., Heckman T. M., Weaver K. A., Dahlem M., 2000, AJ, 120, 2965.
Suchkov A. A., Balsara D. S., Heckman T. M., Leitherer C., 1994, ApJ, 430, 511.
Tenorio-Tagle G., Silich S. A., Kunth D., Terlevich E., Terlevich R., 1999, MNRAS, 309, 332.
Thuan T. X., 1983, ApJ, 268, 667.
Thuan T. X., Martin G. E., 1981, ApJ, 247, 823
Thuan T. X., Sauvage M., 1992, A&AS, 92, 749.
van Bever J., Vanbeveren D., 1998, A&A, 334, 21.
Viallefond F., Thuan T. X., 1983, ApJ, 269, 444.
Weaver R., McCray R., Castor J., Shapiro P., Moore R., 1977, ApJ, 218, 377.
Zimmermann H. U., Becker W., Belloni T., et al., 1997, EXSAS users guide. July 1997 edition.

Table A1. The R XJ numbers, positions, detection significance, count rates and hardness ratios of the 23 sources detected in the *ROSAT* HRI field of view during the 47.7 ks observation of Mrk 33.

Source	R XJ number	RA (2000) (h m s)	Dec. (2000) (° ′ ″)	Sig (σ above background)	Count Rate (10^{-4} ct s^{-1})	HR
X-1	103102.0+542352	10 31 02.0	+54 23 52	7.6	13.8 ± 1.7	0.42 ± 0.12
X-2	103130.2+542101	10 31 30.2	+54 21 01	5.9	5.7 ± 1.1	0.36 ± 0.13
X-3	103136.1+541843	10 31 36.1	+54 18 43	6.8	6.9 ± 1.2	0.59 ± 0.16
X-4	103151.8+542518	10 31 51.8	+54 25 18	6.6	6.1 ± 1.1	0.43 ± 0.13
X-5	103152.0+541728	10 31 52.0	+54 17 28	4.5	3.9 ± 0.9	0.54 ± 0.18
X-6	103153.1+541724	10 31 53.1	+54 17 24	4.6	3.9 ± 0.9	0.42 ± 0.14
X-7	103155.4+541702	10 31 55.4	+54 17 02	7.1	6.7 ± 1.2	0.50 ± 0.16
X-8	103156.6+543036	10 31 56.6	+54 30 36	4.4	2.8 ± 0.8	0.65 ± 0.21
X-9	103205.5+543726	10 32 05.5	+54 37 26	4.2	7.5 ± 1.3	0.38 ± 0.13
X-10	103209.1+543013	10 32 09.1	+54 30 13	9.0	9.2 ± 1.4	0.44 ± 0.12
X-11	103219.4+541234	10 32 19.4	+54 12 34	5.2	6.2 ± 1.1	0.69 ± 0.20
X-12	103219.5+543806	10 32 19.5	+54 38 06	5.0	7.9 ± 1.3	0.73 ± 0.23
X-13	103229.2+542124	10 32 29.2	+54 21 24	4.8	3.9 ± 0.9	0.78 ± 0.25
X-14 (Mrk 33)	103232.0+542402	10 32 32.0	+54 24 02	5.9	5.1 ± 1.0	0.11 ± 0.05
X-15	103233.6+542621	10 32 33.6	+54 26 21	4.8	3.3 ± 0.8	0.32 ± 0.12
X-16	103244.0+543606	10 32 44.0	+54 36 06	8.8	14.3 ± 1.7	0.23 ± 0.07
X-17	103249.0+543409	10 32 49.0	+54 34 09	14.0	21.6 ± 2.1	0.12 ± 0.05
X-18	103249.3+541244	10 32 49.3	+54 12 44	5.0	5.4 ± 1.1	0.69 ± 0.21
X-19	103251.5+541837	10 32 51.5	+54 18 37	4.2	2.6 ± 0.7	0.46 ± 0.15
X-20	103322.8+542523	10 33 22.8	+54 25 23	12.2	13.8 ± 1.7	0.21 ± 0.06
X-21	103341.9+541755	10 33 41.9	+54 17 55	4.1	3.6 ± 0.9	0.53 ± 0.19
X-22	103349.7+541535	10 33 49.7	+54 15 35	6.6	10.8 ± 1.5	0.74 ± 0.20
X-23	103402.6+543019	10 34 02.6	+54 30 19	6.0	11.8 ± 1.6	0.35 ± 0.11